Directed Self-Assembly of Diblock Copolymer Thin Films on Chemically-Patterned Substrates for Defect-Free Nano-Patterning

Yasuhiko Tada,[†] Satoshi Akasaka,[‡] Hiroshi Yoshida,[†] Hirokazu Hasegawa,[‡] Elizabeth Dobisz,[§] Dan Kercher,[§] and Mikihito Takenaka*,[‡]

Materials Research Laboratory, Hitachi Ltd., Hitachi, Ibaraki 319-1292, Japan, Department of Polymer Chemistry, Graduate School of Engineering, Kyoto University, Nishikyo-ku, Kyoto 615-8510, Japan, and San Jose Research Center, Hitachi Global Storage Technologies, 3403 Yerba Buena Road, San Jose, California 95135

Received July 9, 2008; Revised Manuscript Received September 30, 2008

ABSTRACT: We demonstrate that polystyrene-*block*-poly(methyl methacrylate) (PS-*b*-PMMA) can self-assemble in a well-aligned, long-range ordered nanopattern over arbitrarily large areas, commensurate with chemically prepatterned templates prepared by electron beam (EB) lithography. The epitaxially grown cylindrical microdomain formed a defect-free hexagonal lattice although the Chemically-Patterned substrate had some defects in its pattern and errors in pattern position. Furthermore, we demonstrated that the self-assembly process can interpolate points in between the EB generated pattern, thus multiplying the pattern density. The result suggests that the self-assembly of PS-*b*-PMMA can repair the defects of the patterned substrate, while the patterned substrate can align the domain structures of block copolymer into a long-range ordered single array. The developed process, which combines EB lithography and self-assembly of diblock copolymer provides a promising fabrication method for extension of top down-type lithographic capabilities to very high densities.

I. Introduction

Recently, much effort has been devoted to nanofabrication to enhance the performance of microelectronic devices. Smith et al. have demonstrated 35 nm lines and spaces with immersion 193 nm interferometric lithography.[1] Although photolithography is the industry standard high throughput lithography, the resolution requirements have reached beyond the wavelength of light and it is becoming increasingly complicated and expensive to continue further minimizing the resolution.[2] Electron beam (EB) lithography can routinely produce features of 15−25 nm. Under specialized conditions EB lithography can produce features of 2−5 nm.[3−5] However, the application of direct write EB lithography is very limited by its low throughput. To enhance the available lithographic capabilities, self-assembling processes have received much attention.[6−10] In particular, the self-assembly of block copolymers is of interest for this approach.

Diblock copolymers consist of two chemically different immiscible polymers which are joined at the end of each polymer. The diblock copolymers exhibit a wide variety of morphologies ordered by microphase separation. In diblock copolymer melts, separation of the phases can result in microdomain structures such as lamellar, gyroid, *Fddd*, hexagonally packed cylinder, and a body centered lattice of spheres in the equilibrium configuration.[11−15] The equilibrium morphologies depend on the relative volume fraction of diblock copolymers and temperature, while the size of the microdomain structures depend on the molecular weight of the diblock copolymers. The typical sizes of the microdomains are a few tens of nanometers.[12,13]

To realize the full potential of self-assembled structures of block copolymers in thin films for lithographic application, we need to attain long-range order. If self-assembled on a surface without a template guidance, the diblock copolymer forms several crystal-like grains. The crystal type grains are rotated with respect to each other and are separated by a dislocation or grain boundary. To achieve long-range order, some type of guidance during the microdomain formation process is required. For this purpose, several methods such as graphoepitaxy,[16−21] shear flow,[22] electric fields,[23−27] and solvent evaporation[28,29] have been proposed. In this work, we focus on self-assembled diblock copolymer domain structure on substrates Chemically-Patterned with EB lithography.

The effect of a Chemically-Patterned surface on the orientation of microphase separated diblock copolymer was first reported by Rockford et al.[30] The surface prepared by Rockford consisted of alternating stripes of silicon oxide and Au. The surface pattern directed the phase separated structure of Polystyrene-*block*-poly(methyl methacrylate) (PS-*b*-PMMA). Then, Nealey et al. have successfully directed lamellar-[31] and cylinder-forming[32,33] block copolymer self-assembled microdomains in registration with the lithographic pattern defined in the chemically modified surfaces with a one-to-one correspondence.

Recently, Ruiz et al. attained the interpolation of chemical pattern with a 1:2 correspondence by self-assemble of PS-*b*-PMMA. They patterned hexagonally polystyrene-grafted Si substrate by EB lithography and directed the self-assembling process of cylinder-forming PS-*b*-PMMA.[34] Cheng et al. also succeeded in similar interpolation for a stripe pattern.[35] They used a two-layer system consisting of hydrogen silsequioxane (HSQ) layer on the cross-linked film of poly(styrene-*r*-epoxydicyclopentadiene methacrylate). They etched HSQ to form chemically modified stripe patterns and the self-assembling of lamellar-forming PS-*b*-PMMA on the etched substrate succeeded in duplication of the size of the stripe pattern.

Here we investigate how the Chemically-Patterned substrates can control the orientation of the microdomain structure of block copolymer thin films. In particular, we focus on the registration, template dimension match, long-range order, and interpolation of the substrate chemical patterns. The combination of the Chemically-Patterned substrate and the self-assembling of block copolymers is a very promising path to defect-free nanofabrication to 10 nm or below.

* To whom correspondence should be addressed.
[†] Materials Research Laboratory, Hitachi Ltd.
[‡] Department of Polymer Chemistry, Graduate School of Engineering, Kyoto University.
[§] San Jose Research Center, Hitachi Global Storage Technologies.

10.1021/ma801542y CCC: $40.75
Published on Web 11/04/2008

Table 1. Characterization of Polymers Used in This Study[a]

code	polymer	M_n of PS (g/mol)	M_n of PMMA (g/mol)	M_w/M_n
SMMA-1	PS-*b*-PMMA	4.61×10^4	2.10×10^4	1.09
SMMA-2	PS-*b*-PMMA	3.55×10^4	1.22×10^4	1.04
PS-1	PS-OH	9.0×10^2		1.13
PS-2	PS-OH	3.7×10^3		1.08
PS-3	PS-OH	1.0×10^4		1.07

[a] M_n: number-average molecular weight. M_w/M_n: heterogeneity index.

Table 2. Characterization of Polystyrene Graft Layer

PS-OH	XPS C_{1S} intensity (cps)	thickness (nm)	contact angle of PS at 170 °C (deg)
PS-1	8.9×10^3	1.7	24
PS-2	2.7×10^4	5.1	6
PS-3	3.6×10^4	8.7	0

The contents of this paper are as follows: In section II, we describe the substrate and sample preparation, characterization of substrates and samples, and observation method of the self-assembled structure. In section III, we show the results of the self-assembled diblock copolymer structure. We first show the microdomain structure of the diblock copolymers without a template. It is then compared with the microdomain structure of the same diblock copolymers on Chemically-Patterned substrates of systematically varied period. We demonstrate single crystal type microdomain structures on the substrates commensurate with the chemical pattern when the pattern period is almost equal to the equilibrium periodicity of the microdomain structures. The self-assembled patterns correct for defects in the lithographic pattern of the substrate. Subsequently, we show that PS-*b*-PMMA self-assembly can interpolate between features of the chemical template pattern on the substrate, in cases where the template periodicity is close to twice that of the microdomain structure. Finally we conclude our results in section IV.

II. Experimental Section

II-1. Materials. Polystyrene-*block*-poly(methyl methacrylate) (PS-*b*-PMMA) and hydroxy-terminated polystyrene (PS-OH) were purchased from Polymer Source Inc., Quebec, Canada. Characteristics of PS-*b*-PMMA and PS-OH and their code names are listed in Table 1.

II-2. Substrate Preparation. Si substrate surfaces were Chemically-Patterned in the following manner. First the Si substrate was cleaned in a piranha solution at 80 °C for 15min and rinsed in deionized water. Next, a 1.0 wt % PS-OH solution in toluene was spin-coated onto the Si substrate to a thickness of about 50 nm. The grafting of PS on the Si substrate was completed by annealing the PS-OH-coated Si wafer in vacuum at 140 °C for 48 h. Unreacted PS-OH was removed by rinsing the substrate with toluene. We investigated three kinds of grafted PS-OH chemical templates, each with a different molecular weight, as listed in Table 1. Table 1 also shows the molecular weights of the diblock copolymers that were later deposited on the substrates. The measured characteristics of each grafted layer is listed in Table 2. In Table 2, one can see that the average thickness of PS grafted layer increased with molecular weight of PS-OH, and the wettability of PS to the PS grafted surface also increased with the molecular weight of the PS-OH.

Next, the PS-grafted layer was patterned by EB lithography. The patterning process is schematically shown in Figure 1. PMMA resist was spin-coated onto the PS-grafted Si substrate (Figure 1a) to thicknesses of 60 or 85 nm. The 60 nm PMMA was used with diblock copolymer, SMMA-2, to achieve finer period e-beam patterns. The samples were exposed by electron-beam in hexagonal arrays of dots with a Vistec VB6, e-beam lithography system and developed in 3:1 isopropanol:deionized water at 4 °C, under ultrasonic agitation. Since the dots were, e-beam exposed, development removed only the dots in the PMMA. The samples were subsequently etched in a Surface Technology Systems Multiplex

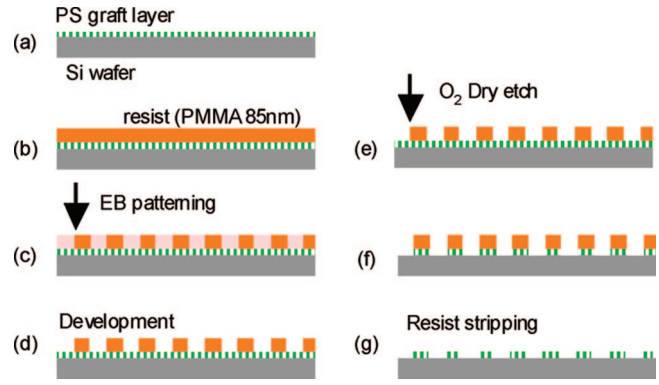

Figure 1. Schematic illustration of EB lithography process to form Chemically-Patterned substrate.

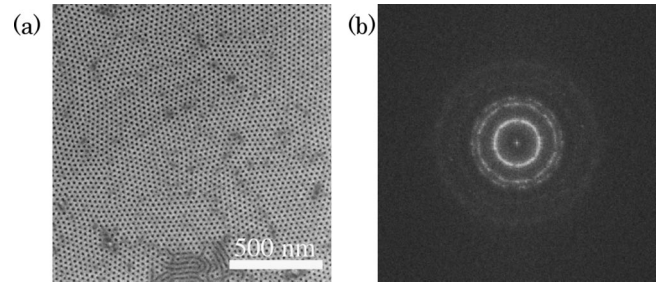

Figure 2. (a) SEM image of SMMA-2 on Si substrate and (b) corresponding 2D-FFT image.

Inductive Coupled Plasma instrument with an O_2 environment. The etching time was short, 5−10 s, so that the PMMA mask remained and only the grafted PS in the holes was selectively reacted with the plasma. The PMMA mask was removed by rinsing the substrate with *N*-methyl-2-pyrolidone and/or toluene, leaving a Chemically-Patterned substrate. The details of the patterns are described below.

II-3. Sample Preparation. Thin films of PS-*b*-PMMA were spin-coated from a dilute solution in toluene. The thickness of the films was controlled by the concentration of the solutions and the spin speed. The spin-coated samples were then annealed at 170 °C for 12 h in vacuum to reach their equilibrium state.

II-4. Scanning Electron Microscope (SEM) Observation. We observed the microdomain structures of PS-*b*-PMMA by using a Hitachi S-4800 field-emission SEM instrument operated at an acceleration voltage of 0.7kV. For contrast between the PMMA and PS phases, the block copolymer specimens were etched by O_2 RIE with a SAMCO RIE-10NR. Since the O_2 RIE preferentially etches the PMMA structures, the dark and bright parts of SEM images correspond to PMMA and PS microdomains, respectively.

III. Results and Discussion

III-1. Microdomain Structures of SMMA-1 and SMMA-2 on a Si Substrate. In order to establish a basis for comparison, the structures of SMMA-1 and SMMA-2 self-assembled on Si without chemical prepatterning was examined. Figure 2a shows the SEM image of the thin film of the SMMA-2 on a Si wafer. In this case, the spin-coated SMMA-2 wafer was annealed at 170 °C for 24 h. The film thickness, t_f,was 45 nm. Here most of part in the image exhibits hexagonally packed cylindrical structures of the PMMA domains oriented perpendicular to the film surface, although there are some regions where PMMA domains oriented parallel to the film surface. However, the extent of the hexagonal lattices on the surface was broken by grain boundaries and the film exhibits a poly granular structure. It should be noted that perpendicular orientation can be formed without any treatment on Si substrate, although we usually need to treat the surface, such as random copolymer or corrugated substrate, to form the perpendicular orientation. This may be

Table 3. Characterization of Patterns Formed with EB Lithography

d_S (nm)	L_s (nm)	d_{obs} (nm)	σ (nm)	
24	28	23.8	5.2	$d_S \approx d_0$ for SMMA-2
26	30	26.0	3.6	$d_S \approx d_0$ for SMMA-2
47	54	47.5	2.2	$d_S \approx 2d_0$ for SMMA-2
48	56	48.4	2.0	$d_S \approx 2d_0$ for SMMA-2
50	58	50.7	2.4	$d_S \approx 2d_0$ for SMMA-2
31	36	31.0	2.8	$d_S \approx d_0$ for SMMA-1
32	36	32.2	2.5	$d_S \approx d_0$ for SMMA-1
61	70	61.3	3.6	$d_S \approx 2d_0$ for SMMA-1
62	72	63.2	3.8	$d_S \approx 2d_0$ for SMMA-1
64	74	64.8	2.6	$d_S \approx 2d_0$ for SMMA-1

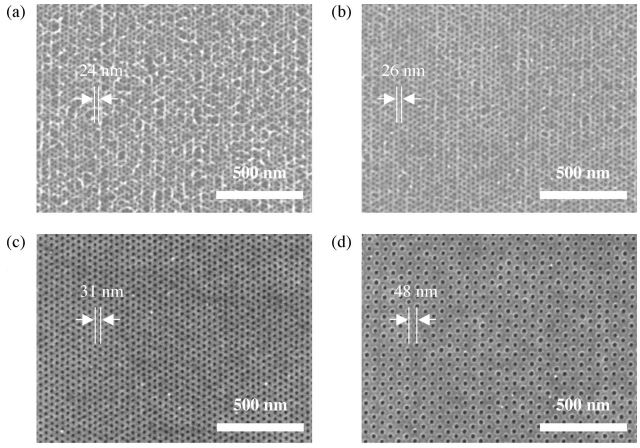

Figure 3. SEM images of patterns of PMMA resist formed with EB lithographic process. (a) $d_S = 24$ nm, (b) $d_S = 26$ nm, (c) $d_S = 31$ nm, and (d) $d_S = 48$ nm.

because the thickness of the sample is suitable for the perpendicular orientation. Actually, the thickness of the parallel orientation regions is thicker than that of the perpendicular orientation. Figure 2b is a 2-dimensional Fast Fourier Transform (2D-FFT) image of the region having perpendicular orientation in the Figure 2a. There are several higher order peaks, with up to sixth order, at $q/q_m = 1$, $\sqrt{3}$, $\sqrt{4}$, $\sqrt{7}$, $\sqrt{9}$, and $\sqrt{12}$, with q_m being the first order peak of the 2D-FFT image. The 2D-FFT image shows that the cylinders were packed regularly on a hexagonal lattice within the grains. However, the 2D-FFT image has isotropic halos with some spots. This pattern suggests a poly crystalline type structure with several hexagonal lattices that are not of the same orientation. From first order peak positions, the intrinsic domain spacing of the self-assembled lattice, d_0, on Si substrate was calculated to be 24 nm. Similar results were obtained for the SMMA-1 thin film on a Si substrate, with d_0 of 32 nm.

III-2. Characterization of Chemically-Patterned Substrate. Two types of substrate patterns were investigated: one with $d_S \approx d_0$, and the other with $d_S \approx 2d_0$, where d_S is the d-spacing specified in the e-beam digital file. The pattern with $d_S \approx 2d_0$ was used to test whether the self-assembling process of PS-*b*-PMMA can interpolate the chemical pattern. A matrix of array patterns, in which the array spacing was varied in 1 nm steps about $d_S \approx d_0$ and $d_S \approx 2d_0$ were written on the substrate. The radius of the dots in the grafted layer was ~10 nm.

The nature and magnitude of defects in the original e-beam patterns were observed through SEM image of the original PMMA mask. The PMMA mask was sputter coated with 1.8 nm of Pt−Pd prior to SEM measurement. Figure 3 shows SEM images of PMMA-mask patterned with $d_S \approx d_0$ for SMMA-1 and SMMA-2 and $d_S \approx 2d_0$ for SMMA-2. While there were several defects in the smaller d_S patterns (Figure 3, parts a and b), there were almost no defects in the larger d_S patterns (Figure 3, parts c and d). A summary of the characterization of the e-beam patterns is given in Table 3. L_S is the nearest lattice distance specified in e-beam pattern file. The parameters, d_S and L_S, are limited to 1 nm integers due to the resolution of the digital grid for the e-beam tool. The parameter d_{obs} is the average d-spacing measured from SEM micrographs, and σ is the standard deviation of measured d-spacings from the average measured value. The final column on the right gives the diblock copolymer and parameter relevant to the e-beam patterns. The method by which d_{obs}, and σ were computed is described in the Appendix.

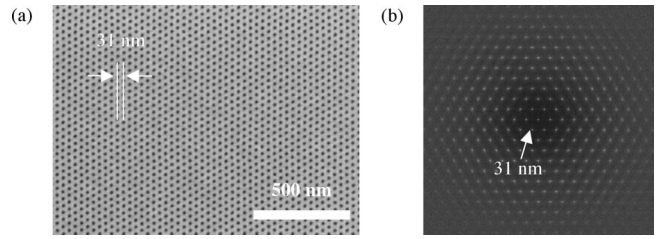

Figure 4. (a) SEM image of self-assembled microdomain structures of SMMA-1 on the Chemically-Patterned substrate with $d_S = 31$ nm and (b) the corresponding 2D-FFT image.

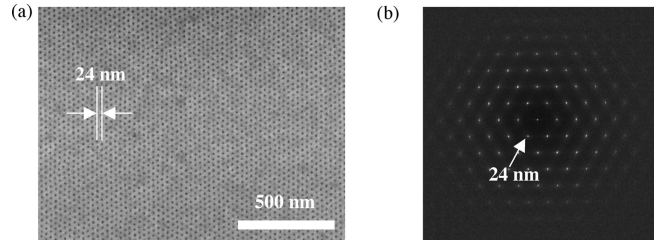

Figure 5. (a) SEM image of self-assembled microdomain structures of SMMA-2 on the Chemically-Patterned substrate with $d_S = 24$ nm and (b) the corresponding 2D-FFT image.

III-3. Microdomain Structures of PS-*b*-PMMA on Chemically-Patterned Substrates with $d_S \approx d_0$. Figure 4a shows the SEM image of the microdomain structures of SMMA-1 on Chemically-Patterned substrate with $d_S = 31$ nm being nearly equal to the d-spacing of SMMA-1, $d_0 = 32$ nm. The thickness of the SMMA-1 film was $t_f = 48$ nm. PS-2 was used as the PS-grafted layer. In the case of the thin film of SMMA-1 on the Si substrate, poly grain structure was observed as shown in Figure 2. On the other hand, the microdomain ordered structure on the Chemically-Patterned substrate did not have any defects and formed a single hexagonal lattice commensurate with the chemical pattern beneath. Moreover, further SEM observation showed that the single hexagonal lattice extended all over the entire 100×100 μm^2 extent of the Chemically-Patterned region. Figure 4b is the 2D-FFT image of the SEM image of Figure 4a. In contrast to the 2D-FFT pattern of the thin film of SMMA-1 on the Si substrate without a Chemically-Patterned template (Figure 2b), the 2D-FFT image of the diblock copolymer ordered on the chemical template exhibits only spots as expected from a single hexagonal lattice, with peaks up to the 11th order. The results show that the microdomain structure formed a well-oriented hexagonal lattice pattern along the Chemically-Patterned substrate with long-range order. The d-spacing calculated from the 2D-FFT was 31 nm, which equaled the d-spacing of the substrate but was slightly smaller than the d-spacing of the SMMA-1 film on the Si substrate. Thus the domain spacing was constrained by the pattern of the substrate.

Figure 5a shows the SEM images of the domain structures of SMMA-2 ($d_0 = 24$ nm) on Chemically-Patterned substrate

Table 4. Quantitative Comparison of d and σ between Patterns Formed with EB Lithography only and That of Self-Assembling Structure of PS-*b*-PMMA on the Chemically-Patterned Substrate

	EB lithography		microdomain	
target d_S (nm)	d_{obs} (nm)	σ (nm)	d (nm)	σ (nm)
24	23.8	5.3	24.1	2.6
48	48.3	2.0	23.8	2.6

with $d_S = 24$ nm. The thickness of the film was 48 nm. PS-2 was used as the PS-grafted layer. Similar to the result of the case of SMMA-1, the cylindrical microdomains on Chemically-Patterned substrate form a single hexagonal lattice commensurate with the lattice of the Chemically-Patterned substrate. In the 2D-FFT image (Figure 5b), a spot pattern of a single hexagonal lattice was found.

To estimate the precision of the hexagonal lattice quantitatively, we calculated the d-spacing d_{obs} and the standard deviation of nearest neighbor lattice distance σ for the vertically oriented cylindrical microdomain structure of the SMMA-2 on the patterns with $d_S = 24$ nm and compared them with those for the patterns formed with EB lithography process as listed in Table 4. The d-spacing for the microdomain structure agrees with that of the e-beam patterns. However, the standard deviation of the lattice spacing, σ, for the microdomain structure was measured to be 2.6 nm, which was half-that of the EB pattern. This results clearly shows that the self-assembling process of the block copolymer can correct patterns formed with EB lithography. Similar result has been found by Ruiz et al.[34] They also investigated the directed self-assembling process of cylinder-forming PS-*b*-PMMA on e-beam pattern and standard deviation of dot placement errors has been found to be much improved in comparison to the e-beam pattern.

III-4. Effects of the Mismatch between d_S and d_0 on the Microdomain Structures on Chemically-Patterned Substrates with $d_S \approx d_0$. As described above, the Chemically-Patterned substrates can control the orientation and spacing of the microdomain structure of the diblock copolymer. We now investigate, the amount of lattice mismatch the lithographically guided self-assembly process can tolerate. Figure 6 shows the SEM and 2D-FFT images of the microdomain structure of SMMA-1 ($d_0 = 32$ nm) on the Chemically-Patterned substrates with different values for d_S. The diblock copolymer film thickness was $t_f = 48$ nm and PS-2 was used as the PS-graft layer. As shown in Figure 6, the regularity and the long-range order of PS-*b*-PMMA become worse with increasing the mismatch between d_S and d_0. In the case of $d_S = 35$ nm, there are some grains and the defects between grains in the SEM image (Figure 6a). Although the 2D-FFT image still shows a hexagonal pattern, reflecting the single orientation of the domain structure, the peaks are broader than those of $d_S = 32$ nm, and the higher order peaks have been lost. The d-spacing of the domain structure the perpendicular orientation. Actually, the thickness of the parallel orientation regions is thicker than that of the perpendicular orientation. Figure e packed regularly on a hexagonal lattice within the grains. However, the 2D-FFT image has isotropic halos with some spots. This pattern suggests a poly crystalline type structure with several hexagonal lattices that are not of the same orientation. From first order peak positions, the intrinsic domain spacing of the self-assembled lattice, d_0, indicating little interaction with substrate surface.

We investigated the azimuthal dependence of the first peak intensity in 2D-FFT image to quantify the distribution of the orientation of the lattice structures. Figure 7 shows the azimuthal angle dependence of the first peak intensity in 2D-FFT image shown in Figures 4 and 6. The peaks become broader with with d_S. The width w obtained by fitting the peaks at 180° with

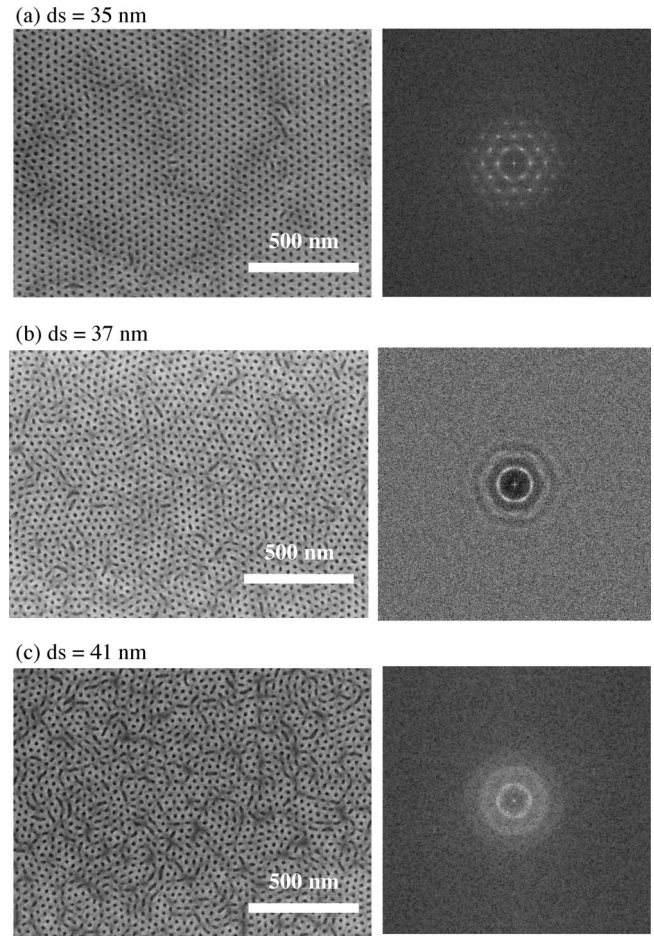

Figure 6. SEM images and corresponding 2D-FFT images for self-assembled microdomain structures of SMMA-1 on the Chemically-Patterned substrate with (a) $d_S = 35$ nm, (b) $d_S = 37$ nm, and (c) $d_S = 41$ nm.

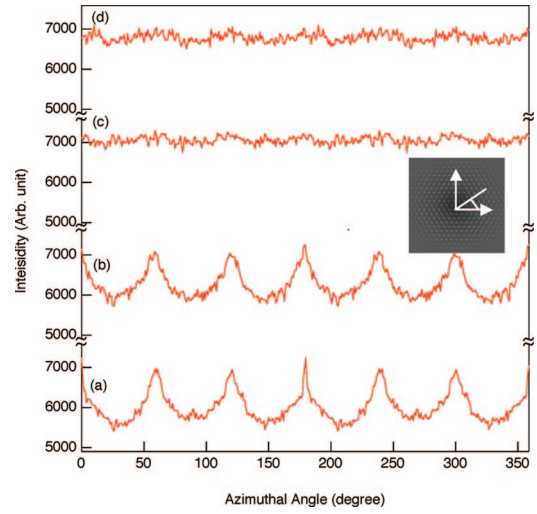

Figure 7. Azimuthal angle dependence of first peak intensity in 2D-FFT image for (a) $d_S = 31$ nm, (b) $d_S = 35$ nm, (c) $d_S = 37$ nm, and (d) $d_S = 41$ nm.

Gaussian function are 3.3° and 9.8° for $d_S = 31$ and 35 nm, respectively, and we can not fit the data for $d_S = 37$ and 41 nm with Gaussian function.

The results are interpreted as a thermodynamic competition between the enthalpy of the lower surface energy in aligning the diblock copolymer domains with the surface chemical pattern, and the loss of conformational entropy as the chains

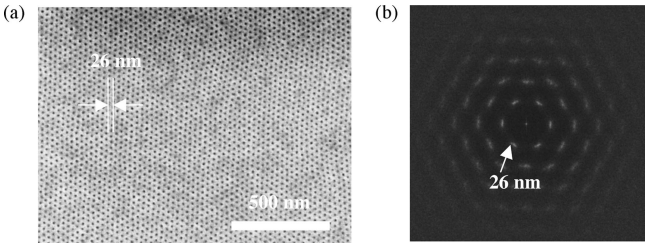

Figure 8. (a) SEM image of self-assembled microdomain structures of SMMA-2 on the Chemically-Patterned substrate with $d_S = 26$ nm and (b) the corresponding 2D-FFT image.

stretch to achieve the lattice spacings of the chemical patterns that increasingly became larger than the equilibrium spacing for that diblock copolymer. Up to a 10% stretch of the lattice spacing ($d_S = 35$ nm), the surface interaction enthalpy dominates and determines d_S of the diblock copolymer. However, the loss of entropy due to the extension of the polymer chains causes the loss of the long-range order so that the thin film can not maintain the single crystal-like structure and multiple grains form to relieve the stress. As the stretch of the lattice spacing becomes 15% ($d_S = 37$ nm), the substrate pattern still tends to control the *d*-spacing of the microdomain structure, but the loss of entropy term becomes comparable and an isotropic microdomain structure with *d*-spacing of 32 nm region appears as a large defects. As the surface pattern stretches d_S by 27% ($d_S = 41$ nm), the surface energy can not make up for the loss of the entropy and the entropy term dominates the control of the *d*-spacing of the microdomain structure. However, the substrate patterns limit the size of the ordered regions with d_0 aligning and prevent any long-range order. Thus, the random orientation is observed in the SEM image.

The SEM image of the microdomain structures of SMMA-2 ($d_0 = 24$ nm) on the Chemically-Patterned substrate with $d_S = 26$ nm, which is an 8% stretch relative to d_0, is shown in Figure 8a. Differing from the case of the Chemically-Patterned substrate with $d_S = 24$ nm (Figure 5), the hexagonal lattice was found to be distorted and the points had a variation in position off the correct lattice points. The 2D-FFT image for $d_S = 26$ nm displayed a spot-like pattern forming a hexagonal lattice indicating that the *d*-spacing of the chemical pattern of 26 nm was still preserved. However, the spots are broader than those of the $d_S = 24$ nm case, suggesting that the hexagonal lattice of the microdomain structure was distorted and the lattice points had some spread in orientations. The lack of the long-range order for $d_S = 26$ nm is caused by the mismatch between d_0 and d_S.

Kim et al. have investigated how the mismatch between d_0 and d_S affects the long-range order of the microdomain structure in lamellar systems of PS-*b*-PMMA.[31] For $d_S < d_0$, although *d*-spacing becomes d_S and there are few defects in the microdomains, the most of part of the microdomains is well registered and epitaxial to the surface pattern. On the other hand, for $d_S > d_0$, there are found to be the two kinds of defects: the formation of herringbone patterns and the unregistered lamellae with d_0. They found the fraction of the unregistered lamellae with d_0 increases with the mismatch. This increase agrees with the case of cylinder-forming systems.

III-5. Effects of Molecular Weight of PS-OH on the Orientation of the Microdomain Structures on Chemically-Patterned Substrates with $d_S \approx d_0$. In the previous sections, the Chemically-Patterned substrate was formed with PS-2, which had a number-average molecular weight (M_n) of 3700. Here we investigate the effect of molecular weight of PS-OH surface on the microdomain structure of the diblock copolymers. Figure 9 shows the SEM images of the microdomain structure of

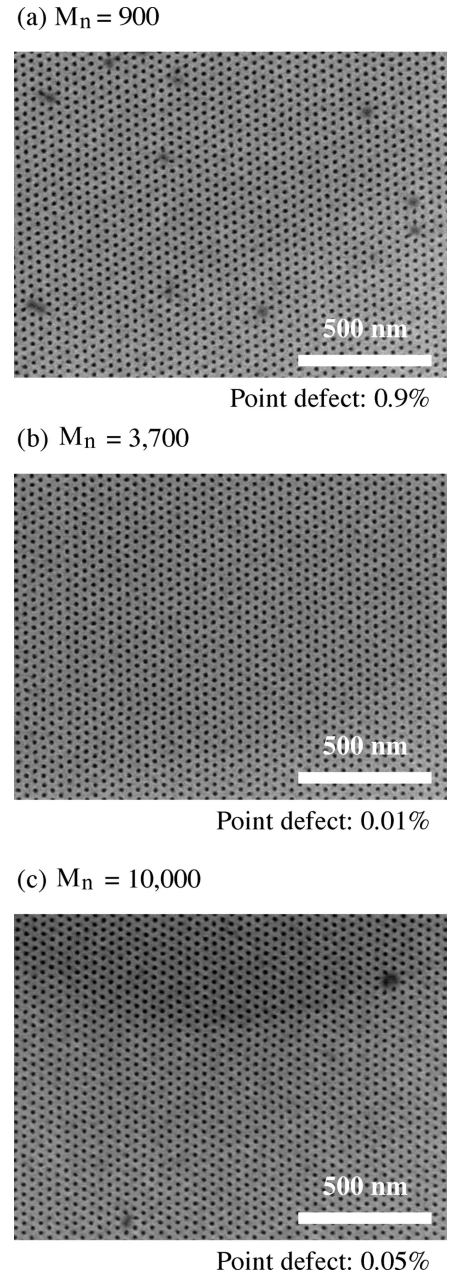

Figure 9. SEM images of the microdomain structures of SMMA-1 on the Chemically-Patterned substrate with (a) PS-1, (b)PS-2, and (c) PS-3. d_S is 32 nm and the film thickness of each sample is 35 nm.

SMMA-1 on Chemically-Patterned substrates with three different molecular weights of PS-OH. Here the $d_S = 32$ nm $= d_0$. The thickness of the films were $t_f = 35$ nm for all samples. We found that the microdomain structures on Chemically-Patterned PS-OH with $M_n = 3700$ had fewer defects the than those on Chemically-Patterned surfaces with the other molecular weight PS-OH films. The percentage of point defects in the lattice was determined from SEM images with 10000 lattice points to be 0.9%, 0.01%, and 0.05% for PS-1, PS-2, and PS-3, respectively. The results indicate that PS-2 (PS-OH with $M_n = 3700$) was optimal as a chemically patterned substrate.

From examination of the contact angles, in Table 2, we can see that PS-1, has the largest contact angle and poorest wetting of the PS. Thus, the imperfection of the coating may cause the defects in lattice structure. Conversely, the substrate with PS-3, which also exhibited more defects than the PS-2 substrate, showed much better wetting of the polystyrene than the PS-2 film. The contradiction between the contact angle and the defects

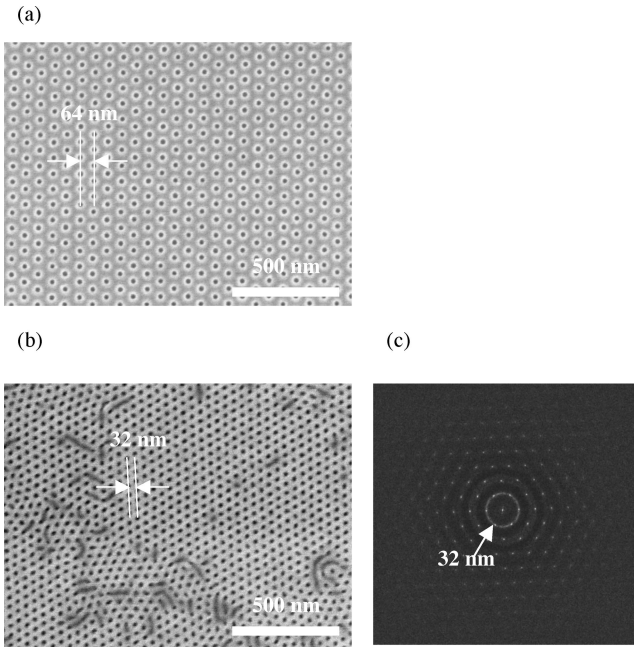

Figure 10. (a) SEM image of PMMA resist pattern with $d_S = 64$ nm, (b) SEM image of the microdomain structure of SMMA-1 on the Chemically-Patterned substrate with $d_S = 64$ nm, and (c) the 2D-FFT image obtained from the SEM image of the microdomain structure.

rate may be due to the fact that the contact angle characterizes wetting in macroscopic scale but does not reflect the heterogeneity of the wetting layer in nanometer scale. The heterogeneity may affect the defect rate. We need to characterize such a heterogeneity of the wetting layer to resolve the contradiction in future work.

III-6. Microdomain Structures of PS-*b*-PMMA on Chemically-Patterned Substrates with $d_S \approx 2d_0$. So far we have demonstrated the conditions under which the self-assembled microdomain structure can replicate and correct a chemical pattern in the substrate. In this section, the concept is taken at step further. We demonstrate that the self-assembled microdomain structure can interpolate patterns in which the substrate was Chemically-Patterned with $d_S \approx 2d_0$. Figure 10 shows the SEM images of (a) PMMA resist pattern with $d_S = 64$ nm, (b) the microdomain structure of SMMA-1 ($d_0 = 32$ nm) on the Chemically-Patterned substrate with $d_S = 64$ nm, and (c) the corresponding 2D-FFT image. The film thickness was $t_f = 48$ nm and PS-2 was used as the PS-grafted Chemically-Patterned layer. We found a hexagonal lattice in most of the area in the SEM image but several cylinders oriented parallel to the substrate surface were also observed. 2D-FFT image exhibits a spots-like pattern with several higher order spots, but a halo ring was also observed, reflecting the defects. Therefore, in the case in which $d_S = 64$ nm $= 2d_0$, the microdomain structures were well-directed by the substrate with long-range order but that there were some defects in the microdomain structures.

Figure 11 shows the SEM images of the microdomain structures of SMMA-1 ($d = 32$ nm) on Chemically-Patterned substrate with (a) $d_S = 61$ nm, (b) $d_S = 62$ nm, and the corresponding 2D-FFT images. Again the thickness of the film was $t_f = 48$ nm. PS-2 was used as the PS-grafted layer. In each SEM image, we found several cylinders oriented parallel to the substrate surface, although the most of the SEM imaged regions show hexagonal lattices, suggesting the lack of the long-range order. In the case of $d_S = 61$ nm, the 2D-FFT image exhibited a hexagonal spot pattern with limited higher order spots, indicating that the grain size of hexagonal lattice was not large. On the other hand, 2D-FFT images for $d_S = 62$ nm and $d_S =$ 64 nm (Figure 10c), exhibit halo rings with the spots. The higher order peaks were observed more clearly than those in the 2D-FFT image of $d_S = 61$ nm. Thus, the grain sizes of the $d_S = 62$ nm and $d_S = 64$ nm (Figure 10(b)) patterns were larger than that for the $d_S = 61$ nm pattern. The d-spacing estimated from all three 2D-FFT images were 32 nm and were independent of d_S. Since the azimuthal angle dependences of the first order peak intensity for $d_S = 61$ nm, 62 and 64 nm do not have distinct peaks, we can not characterize the distribution.

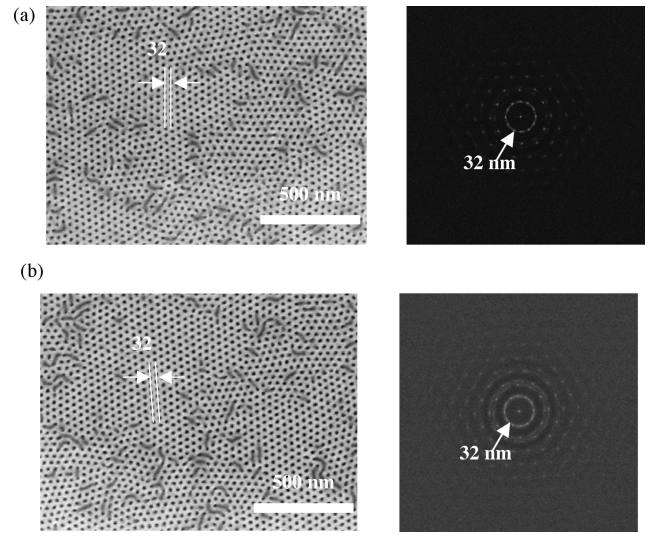

Figure 11. SEM images and corresponding 2D-FFT images for self-assembled microdomain structures of SMMA-1 on the Chemically-Patterned substrate with (a) $d_S = 61$ nm, (b) $d_S = 62$ nm.

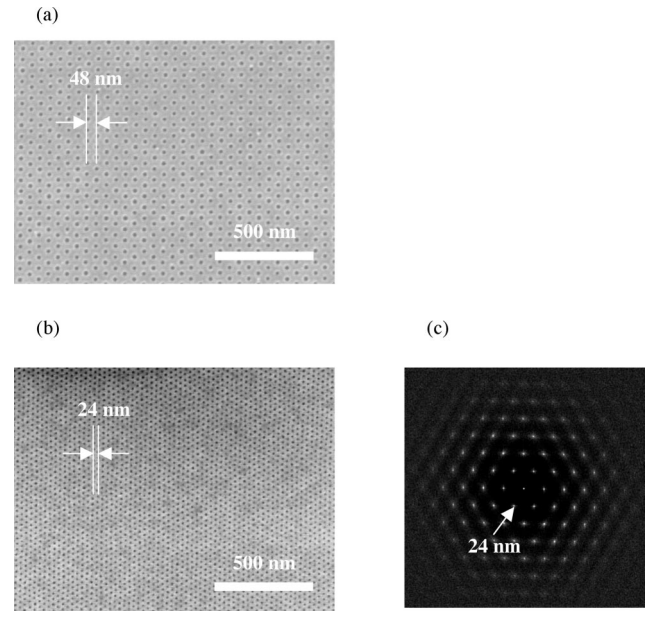

Figure 12. (a) SEM image of PMMA resist pattern with $d_S = 48$ nm, (b) SEM image of the microdomain structure of SMMA-2 on the Chemically-Patterned substrate with $d_S = 48$ nm, and (c) the 2D-FFT image obtained from the SEM image of the microdomain structure.

Figure 12 shows the SEM images of (a) PMMA resist pattern with $d_S = 48$ nm, (b) the microdomain structure of SMMA-2 ($d_0 = 24$ nm) on the Chemically-Patterned substrate with $d_S = 48$ nm, and (c) the corresponding 2D-FFT image. The film thickness was $t_f = 38$ nm and PS-2 was used for PS-graft layer. In contrast to the results for SMMA-1 described above, we obtained defect-free and single-crystal-like microdomain structure on the substrate. The corresponding 2D-FFT images exhibit

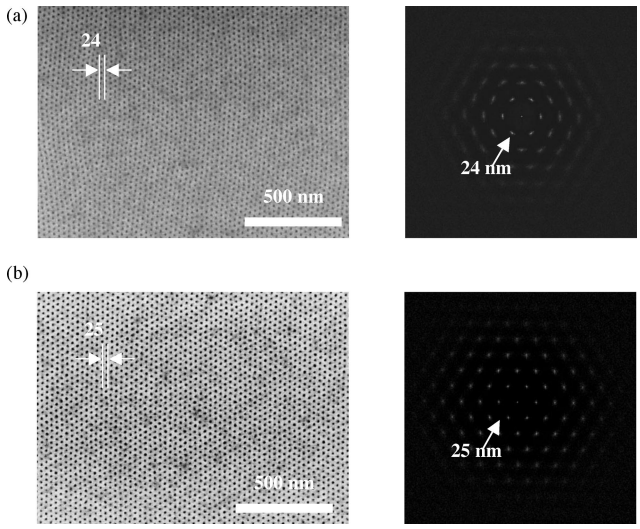

Figure 13. SEM images and corresponding 2D-FFT images for self-assembled microdomain structures of SMMA-2 on the Chemically-Patterned substrate with (a) $d_S = 47$ nm, and (b) $d_S = 50$ nm.

spot-like patterns aligned to the chemical patterns with higher-order peaks. This result indicates that the self-assembling of PS-*b*-PMMA can well interpolate the chemical patterns formed with EB lithography process. As already mentioned above, Ruiz et al. recently reported that the interpolation by the self-assembling of PS-*b*-PMMA can be done successfully on the chemical patterns formed with an EB lithography process.[34] Both results clearly show that directed self-assemble of block copolymers can duplicate the density of nanopatterns.

Figure 13 shows the SEM images of the microdomain structures of SMMA-2 on a Chemically-Patterned substrate with (a) $d_S = 47$ nm, and (b) $d_S = 50$ nm, and the corresponding 2D-FFT images. The thickness of the film was $t_f = 38$ nm and PS-2 was used. In the case of $d_S = 47$ nm, the SEM image did not exhibit large defects but the orientation of hexagonal lattices was slightly distorted. The 2D-FFT image did not show higher order peaks. The estimated *d*-spacing from the 2D-FFT image was 24 nm in agreement with $d_0 = 24$ nm, which was slightly larger than half of 47 nm. If the microdomain structure was constrained by the Chemically-Patterned substrate, a *d*-spacing of 23.5 nm would be expected.

In the cases of $d_S = 50$ nm and $d_S = 48$ nm, single hexagonal lattices were formed in the microdomain structures as shown in the SEM images of Figures 12b and 13b. The corresponding 2D-FFT images exhibited spot-like patterns in the orientation aligned to that of the chemical patterns with higher-order peaks. These results show that self-assembling of PS-*b*-PMMA can interpolate between lattice points in the substrate template, even when a slight mismatch is present, when $d_S > 2d_0$.

We investigated the azimuthal dependence of the first peak intensity in 2D-FFT image shown in Figures 12 and 13. The width *w* obtained by fitting the peaks at 180° with Gaussian function are 4.9°, 3.0° and 3.1° for $d_S = 47$ nm, 48 nm, and 50 nm, respectively.

The interesting point is that the interpolation can be done successfully when $d_S > 2d_0$, while the self-assembly can not interpolate the patterns of the substrate when d_S is slightly smaller than $2d_0$. A similar amount of conformational entropy loss is expected from compression, for $d_S < 2d_0$, as from extension, for $d_S > 2d_0$ in PS chains. However, the extension of polymer chains causes increased surface contact area between PS chains and the PS-graft layer, which should result in a further decrease in the interfacial energy. A compression would have the opposite effect, to the extension, with less surface area of the PS-grafted layer exposed to the polystyrene and an increase in surface energy. Therefore we would not expect interpolation to work at $d_S < d_0$ or when d_S is slightly smaller than $2d_0$.

To estimate the accuracy of the hexagonal lattice quantitatively, we calculated the *d*-spacing and the standard deviation for the microdomain structure of the SMMA-2 on the patterns with $d_S = 48$ nm and compared them with the substrate patterns formed with EB lithography and the results of the self-assembled patterns for $d_S = d_0$. The results are summarized in Table 4. The *d*-spacing of the microdomain structure was almost half of the *d*-spacing of the pattern and agreed with the *d*-spacing of the microdomain structure for 1:1 correspondence. The results indicate that self-assembly interpolated the pattern of the substrate. The standard deviation of the interpolated pattern was slightly worse than that of the $2d_0$ patterned substrate but was identical to that of the microdomain structure on the $d_S \approx d_0$ patterned substrate. This indicates that the regularity of lattice structure is controlled by the self-assembled microdomains and that self-assembly is a viable process to quadruple lithographic pattern density resolution.

As described above, the interpolation in 1:2 correspondence can successfully performed for $d_0 = 24$ nm but can not be done well for $d_0 = 32$ nm. The following discussion could explain the difference between $d_0 = 24$ nm and $d_0 = 32$ nm: For the interpolation, the PMMA cylinders at the interpolation points have to stand perpendicular to the substrate on PS-graft layer. If the segregation between PMMA cylinders and PS-graft layers is strong, the cylinders can not stand perpendicular to the substrate on the PS-graft layer. The segregation strength is usually quantified by χN, which depends on the Flory−Huggins interaction parameter per monomer χ, and polymerization index of polymers *N*. Since the molecular weight of PMMA in SMMA-1 is larger than that in SMMA-2, the segregation between PMMA chains and PS-graft layer for SMMA-1 is stronger than that of SMMA-2. Thus the stability of PMMA cylinders oriented perpendicular to the substrate for $d_0 = 32$ nm will be worse compared to that for $d_0 = 24$ nm. Since density multiplication is most applicable to the densest of patterns the effect of molecular weight on the ability to interpolate is favorable to lithographic applications.

III-7. Effects of the Film Thickness on the Orientation of the Microdomain Structure on the Chemically-Patterned Substrate with $d_S \approx 2d_0$. In the previous section, we proved that the self-assembling process of the diblock copolymer can interpolate the Chemically-Patterned lattice points so that a single crystal-like lattice can be formed on the Chemically-Patterned substrate with $d_S \approx 2d_0$ and thus multiply the pattern density. Here we examine the effects of film thickness t_f on the orientation of the microdomain structures for $d_S \approx 2d_0$.

Figure 14 shows effects of film thickness, t_f, on the orientation of the microdomain structures of SMMA-1 ($d_0 = 32$ nm) on the substrate with $d_S = 64$ nm. In the case where the film thickness was $t_f = 32$ nm, which is almost equal to d_0, the interpolation was not observed in most of the area. PMMA cylinders were registered on the Chemically-Patterned lattice points with their orientation perpendicular to the substrate, but PS formed hexagonal shaped domains surrounded by the PMMA continuous phase in between the lattice points. On the other hand, when film thickness was adjusted to $t_f = 48$ nm, which is almost equal to $(3/2)d_0$, the PMMA cylinders stand perpendicular to the surface of the substrate in between the Chemically-Patterned lattice points as well as on the lattice points, and the interpolation by the self-assembling of PS-*b*-PMMA can be observed over most of the area in the SEM image (Figure 10 b). Interpretation of structure observed for $t_f = 32$ nm and influence of film thickness on the interpolation are discussed below.

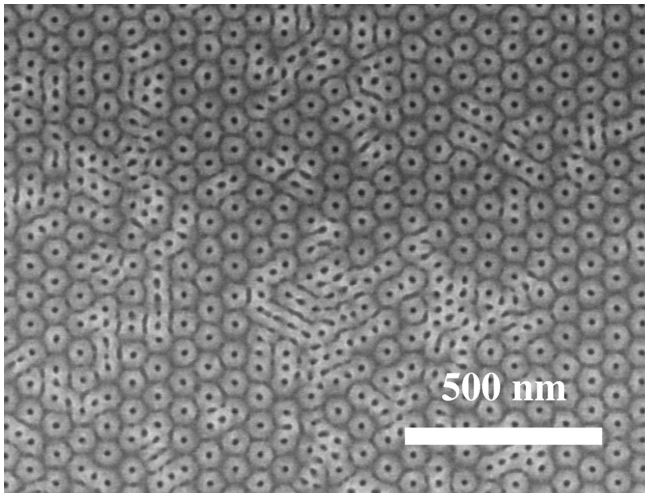

Figure 14. SEM images of the microdomain structures of SMMA-1 on the Chemically-Patterned substrate with $d_S = 62$ nm and the film thickness of 32 nm.

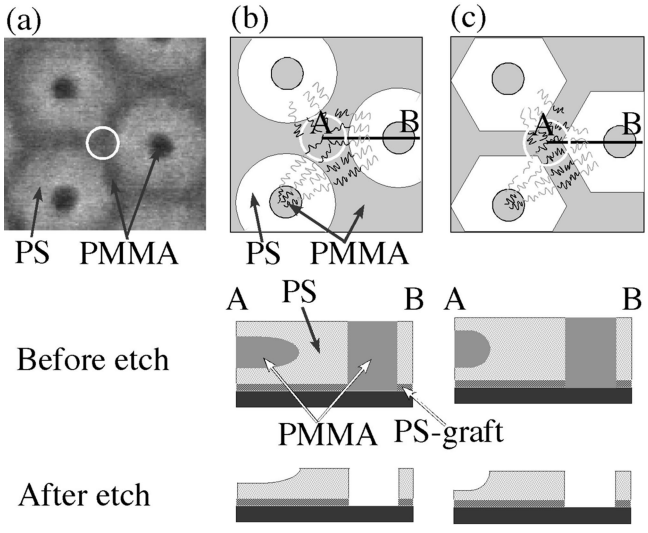

Figure 15. (a) Enlarged SEM images of hexagonal structure of PS domains. (b) Chain packing model for circular PS domain surrounding the perpendicularly oriented cylinder on the chemical lattice point, and cross sections of the thin film along A to B before and after etch for SEM observation. (c) Chain packing model for hexagonal PS domain surrounding the perpendicularly oriented cylinder on the chemical lattice point, and cross sections of the thin film along A to B before and after etch for SEM observation. White circles in parts a−c correspond to junction regions of the PMMA continuous phase, where PMMA domains connected each other.

When $t_f = 32$ nm, the PMMA domains on Chemically-Patterned lattice points (which appear as black dots in Figure 14), were surrounded by lighter PS domains as mentioned above. The shape of surrounding PS domains were mainly hexagonal as can be clearly seen in the enlarged SEM image presented in Figure 15a. Between the PS domains, PMMA formed a continuous phase, which appeared as a gray phase in Figure 14 and Figure 15a. We can speculate the origin of this hexagonal structure as follows: The PS-*b*-PMMAs used in this study forms PMMA cylinders in PS matrix as their equilibrium structure in bulk state, and they tend to form cylindrical microdomains rather than lamellae or plate-like structures even in thin films. PS chains of PS-*b*-PMMA tend to preferentially wet the PS-graft layer. PS chains are also favored at the free surface.[36,21] Therefore, in the region between the Chemically-Patterned lattice points, the PMMA forms a continuous phase in between two PS layers, one facing the free surface and one facing the PS-graft layer, as presented in the schematic cross section in Figure 16a. If the PS domains surrounding the vertical PMMA cylinders were to form concentric cylinders as shown in Figure 15b, the PMMA junctions in the continuous phase region (indicated by gray in Figure 15b) would becomes platelet shape at the junctions of the PMMA cylinders. This shape would cause a loss of the conformational entropy of PMMA chains. If the PS domains form hexagons as shown in Figure 15c, the PMMA at the junction region in the continuous phase region can form a structure closer to cylinders. In this case, the loss of conformational entropy of joining PMMA chains would be less than the case where joining PMMA chains form platelets. Although PS chains looses the conformational entropy in this case by expanding the PS domains to form hexagons, the enthalpic term due to the decrease in the contact area between PS chains and PMMA chains can compensate the loss of the entropy. Also the PS would be in contact with both surfaces and lower the surface energy. To confirm the discussion on the effects of the thickness on the orientation of the microdomains as described above, we need to investigate the cross sectional images of the samples. The investigation remains as a future work.

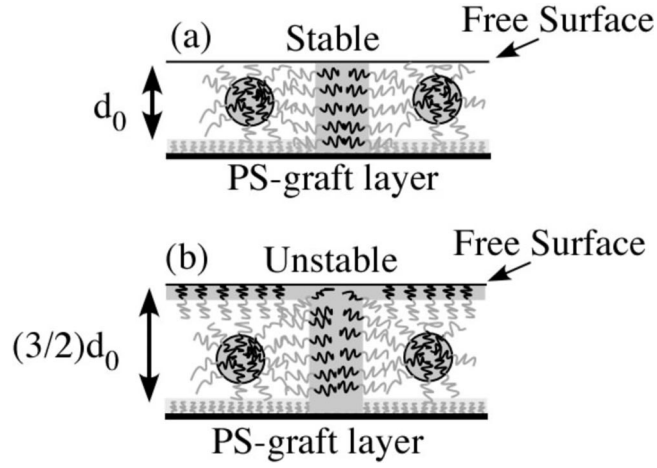

Figure 16. Schematic illustration of chains of PS and PMMA for (a) $t_i = d_0$ and (b) $t_i = (3/2)d_0$. The substrate is a PS-graft layer.

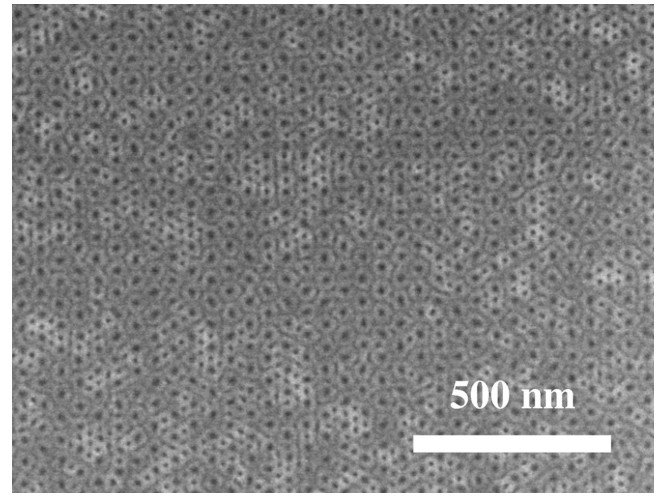

Figure 17. SEM images of the microdomain structures of SMMA-2 on the Chemically-Patterned substrate with $d_S = 48$ nm and the film thickness of 25 nm.

In the case of the thicker block copolymer film, $t_f = 48$ nm $= (3/2)d_0$, the PMMA cylinders stand perpendicular to the PS-grafted surface of the substrate and successfully the interpolate the points between the Chemically-Patterned lattice points. This is also driven by surface chemistry as shown in Figure 16. In the thicker film

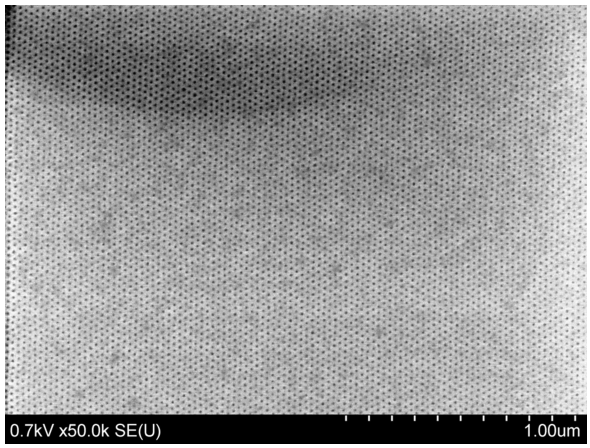

Figure 18. SEM image of microdomain structure of block copolymers.

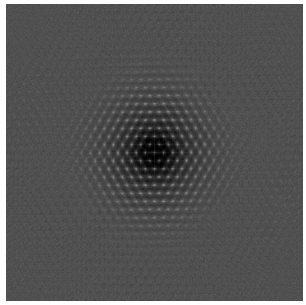

Figure 19. 2D-FFT image of Figure 18.

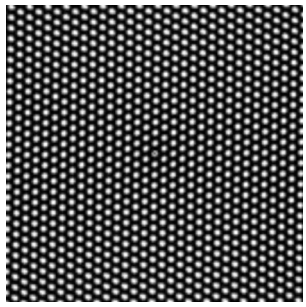

Figure 20. Autocorrelation patterns of Figure 18.

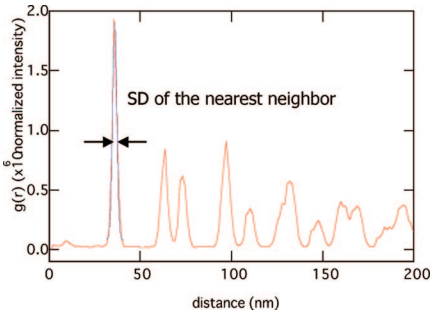

Figure 21. Radial distribution function $g(r)$ plotted as a function of the distance r.

case, shown in Figure 16b, if the cylinders were oriented parallel to the substrate surface, sterical filling of the film thickness would bring the PMMA chains in contact with the free surface. This situation is energetically unfavored.[36,21] The contact area between the two surfaces and the PMMA cylinders is minimized if the PMMA cylinders are perpendicular to the surface. Thus, the PMMA cylinders tend to orient perpendicular to the substrate surface and interpolate the chemical pattern. If on the other hand, t_f is equal to d_0, as in Figure 16 a, the PMMA cylinders can orient parallel to the substrate with the PS contacting both surfaces.

A similar tendency was observed for SMMA-2 as shown in Figure 17. In the case when the film thickness was $t_f = 25$ nm, which is equal to d_0 of SMMA-2 (Figure 17), the interpolation was not observed in all regions and PMMA domains on substrate template were surrounded by hexagonal PS domains. The PMMA formed a continuous phase between the PS domains as observed with SMMA-1 with $t_f = 32$ nm. In the case for $t_f = 38$ nm, which is equal to $(3/2)d_0$, the single crystal-like hexagonal lattice was completed by the interpolation as shown in Figure 12b. The enhancement of the interpolation is caused by the minimization of the surface energy for perpendicular PMMA cylinders, as in the case of SMMA-1 with $t_f = 48$ nm. The results show that the perpendicular orientation of the PMMA cylinders in substrate surface pattern interpolation is strongly controlled by the film thickness.

IV. Conclusion

We have investigated how the Chemically-Patterned substrate affects the microdomain structure of block copolymers on the substrate. First, we characterized the EB patterned substrate and found the imperfection in patterns increases with decreasing *d*-spacing. We investigated the microdomain structure of PS-*b*-PMMA, on the Chemically-Patterned substrate with *d*-spacing of the pattern being nearly equal to the intrinsic *d*-spacing of the PS-*b*-PMMA. The epitaxially grown cylinder structures are well aligned in a defect-free hexagonal lattice, although the Chemically-Patterned substrate pattern has defects. Self-assembly of PS-*b*-PMMA can repair the pattern defects of the patterned substrate. At the same time, the Chemically-Patterned substrate forms a template to align the orientation of the domain structures of block copolymer into a long-range ordered single crystal structure not achievable by self-assembly alone. We have also investigated the effects of the molecular weight of PS-OH of the patterns and found PS-2 having $M_n = 3700$ is most suitable for making defect-free microdomain structures. We successfully demonstrated that self-assembly of the PS-*b*-PMMA can interpolate points in between the chemical lattice pattern generated by EB lithography, thus multiplying the pattern density. We have found that the diblock copolymer film thickness plays an important role on the ability of the microdomains to interpolate the lithographic pattern.

The combined process of nanolithography and self-assembly of diblock copolymers provides a promising fabrication method for extension of top down-type lithographic capabilities to very high densities.

Acknowledgment. H.Y. gratefully thanks Dr. Ricardo Ruiz, Dr. Thomas R. Albrecht (Hitachi Global Storage Technologies) and Professor Paul F. Nealey (University of Wisconsin) for their useful discussions.

Appendix

Here we shall show the procedure to estimate the standard deviation σ of the distance between the centers of the PMMA domains. First, we determined the center of PMMA domain from the SEM image (Figure 18) and applied FFT to the obtained distribution of the centers (Figure 19). Then, we calculated an autocorrelation 2D pattern (Figure 20) from the 2D-FFT pattern, circularly averaged the autocorrelation 2D pattern to obtain a radial distribution function $g(r)$ (Figure 21). By fitting the first order peak reflecting the distribution of the distance between nearest neighbor centers of gravity with Gaussian function we estimated the standard deviation σ.

References and Notes

(1) Smith, B. W.; Bourov, A.; Kang, H.; Cropanese, F.; Fan, Y.; Lafferty, N.; Zavyalova, L. *Proc. SPIE* **2004**, *273*, 5377.
(2) Terris, B. D.; Thomson, T. *J. Phys. D: Appl. Phys.* **2005**, *38*, R199.
(3) Muray, A.; Scheinfein, M.; Isaacson, M.; Adesida, I. *J. Vac. Sci. Technol.* **1985**, *B3*, 367.
(4) Yasin, S.; Hasko, D. G.; Ahmed, H. *Microelectron. Eng.* **2002**, *61*−*62*, 754.
(5) Yang, X. M.; Xiao, S.; Wu, W.; Xu, Y.; Lee, K.; Kuo, D.; Weller, D. *J. Vac. Sci. Technol.* **2007**, *B25*, 2202.
(6) Park, C.; Yoon, J.; Thomas, E. L. *Polymer* **2003**, *44*, 6725.
(7) Hamley, I. W. *Angew. Chem., Int. Ed.* **2003**, *42*, 1692.
(8) Segalman, R. A. *Mater. Sci. Eng. Res.* **2005**, *48*, 191.
(9) Hawker, C. J.; Russell, T. P. *MRS Bull.* **2005**, *30*, 952.
(10) Stoykovich, M. P.; Nealey, P. F. *Mater. Today* **2006**, *9*, 20.
(11) Khandpur, A. K.; Forster, S.; Bates, F. S.; Hamley, I. W.; Ryan, A. J.; Bras, W.; Almdal, K.; Mortensen, K. *Macromolecules* **1995**, *28*, 8796.
(12) Bate, F. S.; Fredrickson, G. H. *Annu. Rev. Phys. Chem.* **1990**, *41*, 525.
(13) Hashimoto, T., In *Thermoplastic Elastmers*; Legge, N. R., Holden, G., Schroeder, H. E., Eds.; Hanser: Vienna, 1996.
(14) Matsen, M. W.; Schick, M. *Phys. Rev. Lett.* **1994**, *72*, 2660.
(15) Takenaka, M.; Wakada, T.; Akasaka, S.; Nishitsuji, S.; Saijo, K.; Shimizu, H.; Kim, M. I.; Hasegawa, H. *Macromolecules* **2007**, *40*, 4399.
(16) Black, C. T.; Guarini, K. W.; Milkove, K. R.; Baker, S. M.; Russell, T. P.; Tuominen, M. T. *Appl. Phys. Lett.* **2001**, *79*, 409.
(17) Segalman, R. A.; Yokoyama, H.; Kramer, E. J. *Adv. Mater.* **2001**, *13*, 1152.
(18) Sundrani, D.; Sibener, S. J. *Macromolecules* **2002**, *35*, 8531.
(19) Cheng, J. Y.; Mayes, A. M. *Nat. Mater.* **2004**, *3*, 823.
(20) Xiao, S. G.; Yang, X. M.; Edwards, E. W.; La, Y. H.; Nealey, P. F. *Nanotechnology* **2005**, *16*, S324.
(21) Chen, F.; Akasaka, S.; Inoue, T.; Takenaka, M.; Hasegawa, H.; Yoshida, H. *Macromol. Rapid Commun.* **2007**, *28*, 2137.
(22) Angelescu, D. E.; Waller, J. H.; Adamson, D. H.; Deshpande, P.; Chou, S. Y.; Register, R. A.; Chaikin, P. M. *Adv. Mater.* **2004**, *16*, 1736.
(23) Thurn-Albrecht, T.; Scotter, J.; Kastle, G. A.; Emley, N.; Shibauchi, T.; Krusin-Elbaum, L.; Guarini, K.; Black, C. T.; Tuominen, M. T.; Russell, T. P. *Science* **2000**, *290*, 2126.
(24) Mansky, P.; DeRouchey, J.; Russell, T. P.; Mays, J.; Pitsikalis, M.; Morkved, T.; Jaeger, H. *Macromolecules* **1998**, *31*, 4399.
(25) Mansky, P.; Liu, Y.; Huang, E.; Russell, T. P.; Hawker, C. *Science* **1997**, *275*, 1458.
(26) Morkved, T. L.; Lu, M.; Urbas, A. M.; Ehrichs, E. E.; Jaeger, H. M.; Mansky, P.; Russell, T. P. *Science* **1996**, *273*, 931.
(27) Xu, T.; Zvelindovsky, A. V.; Sevink, G. J. A.; Lyakhova, K. S.; Jinnai, H.; Russell, T. P. *Macromolecules* **2005**, *38*, 10788.
(28) Kim, S. H.; Misner, M. J.; Russell, T. P. *Adv. Mater.* **2004**, *16*, 2119.
(29) Kim, S. H.; Misner, M. J.; Xu, T.; Kimura, M.; Russell, T. P. *Adv. Mater.* **2004**, *16*, 226.
(30) Rockford, L.; Liu, Y.; Mansky, P.; Russell, T. P.; Yoon, M.; Mochrie, S. G. J. *Phys. Rev. Lett.* **1999**, *82*, 2602.
(31) Kim, S. O.; Solak, H. H.; Stoykovich, M. P.; Ferrier, N. J.; dePablo, J. J.; Nealey, P. F. *Nature* **2003**, *424*, 411.
(32) Edwards, E. W.; Stoykovich, M. P.; Solak, H. H.; Nealey, P. F. *Macromolecules* **2006**, *39*, 3598.
(33) Welander, A. M.; Kang, H.; Stuen, K. O.; Solak, H. H.; Müller, M.; de Pablo, J. J.; Nealey, P. F. *Macromolecules* **2008**, *41*, 2759.
(34) Ruiz, R.; Kang, H.; Detcheverry, F. A.; Dobisz, E.; Kercher, D. S.; Alberecht, T. R.; de Pablo, J. J.; Nealey, P. F. *Science* **2008**, *321*, 936.
(35) Cheng, J. Y.; Rettner, C. T.; Snaders, D. P.; Kim, H. C.; Hinsberg, W. D. *Adv. Mater.* **2008**, *20*, 3155.
(36) Russell, T. P.; Coulon, G.; Deline, V. R.; Miller, D. C. *Macromolecules* **1989**, *22*, 4600.

MA801542Y